Interfacially Driven Instability in the Microchannel Flow of a Shear-Banding Fluid

P. Nghe,[1] S. M. Fielding,[2] P. Tabeling,[1] and A. Ajdari[3]

[1]*Laboratoire Microfluidique, MEMS et Nanostructures, UMR Gulliver CNRS-ESPCI 7083, France*

[2]*Department of Physics, University of Durham, Science Laboratories, South Road, Durham. DH1 3LE, United Kingdom*

[3]*Laboratoire Physico-Chimie Theorique, UMR Gulliver CNRS-ESPCI 7083, France*

(Received 22 February 2010; published 17 June 2010)

Using microparticle image velocimetry, we resolve the spatial structure of the shear-banding flow of a wormlike micellar surfactant solution in a straight microchannel. We reveal an instability of the interface between the shear bands, associated with velocity modulations along the vorticity direction. We compare our results with a detailed theoretical study of the diffusive Johnson-Segalman model. The quantitative agreement obtained favors an instability scenario previously predicted theoretically but hitherto unobserved experimentally, driven by a normal stress jump across the interface between the bands.

DOI: 10.1103/PhysRevLett.104.248303 PACS numbers: 83.80.Qr, 47.50.−d, 83.60.Wc, 83.85.Ei

Shear banding—the coexistence of bands of differing shear rate at uniform stress—is widely reported in the flow of surfactants, colloids, liquid crystals, polymers, foams, granular matter and biphasic systems [1–3]. In recent years, it has been realized that complex spatiotemporal patterns and dynamics are generic features of these banded flows [4]. Distinct from the existing class of instabilities that has been intensively studied for bulk (unbanded) viscoelastic flows in curved geometries [5], this opens up the exciting prospect of new instability and patterning scenarios. This Letter aims to show that such a category of novel instabilities indeed exists, by exploring the flow of a shear-banding wormlike micellar surfactant in a straight microchannel. Instabilities such as these are relevant to applications of surfactants in, e.g., oil recovery and personal care products, and for lab-on-chip technologies such as microfluidic rheometry [6,7].

Significant progress in the experimental study of shear-banding flows has been achieved using local imaging techniques such as NMR [8], dynamic light scattering [9] or ultrasound velocimetry [10], with a typical spatial resolution of 50 μm across $\approx$1 mm gaps in Couette rheometers. Later work using particle image velocimetry with an enhanced 1 μm resolution demonstrated shear banding along the smallest dimension ($\approx$100 μm) in microchannel Poiseuille flow [6,7]. Thanks to such techniques, observations of *temporal* fluctuations of shear-banded flows are now quite widespread in curved Couette geometries [4]. Recent 2D light scattering measurements have further revealed *spatial* interfacial modulations [11,12] suggestive of a viscoelastic Taylor-Couette-like instability arising from the interplay between cell curvature and large normal stresses in the high shear band [13]. Meanwhile, theoretical analysis of shear banding in planar Couette flow has predicted a different instability, triggered by a jump in normal stress across the interface between the bands [14,15]. These studies thus suggest the existence of (at least) two different instability mechanisms that can lead to 2D patterning in shear-banded flows. Here we report the first experimental observation of the second (interfacial) kind of instability, in a planar microchannel.

We perform local velocity measurements in the pressure driven flow of a semidilute wormlike micellar surfactant through a rectilinear microchannel of rectangular cross section [Fig. 1(a)]. We start by reporting a technical advance in such flow characterization, in which we achieve the imaging of two velocity components (stream x and lateral z projections) along the three dimensions of space with excellent spatial resolution. This allows us then to report spatial velocity modulations that indicate an instability of the interface between the shear bands. This is characterized by a downstream evolution from (near the inlet) a smooth interface between the bands, to (downstream) interfacial undulations with a wave vector along the vorticity axis z, i.e., along the width of the channel. We report the wavelength and amplitude of the fully developed instability as a function of applied pressure gradient. We

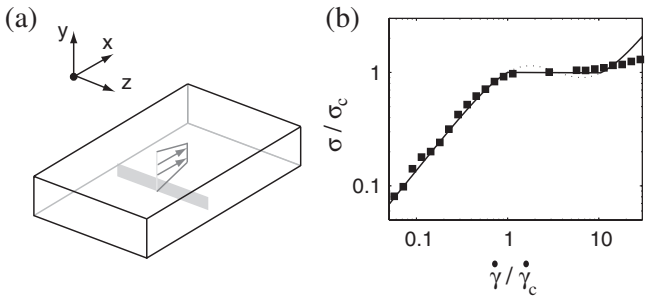

FIG. 1. (a) Sketch of the microchannel and coordinate system with a local 1D shear-banded flow profile. The grey rectangle represents a typical (y, z) area for a velocity imaging such as Fig. 2(a). (b) Stress *vs.* strain rate relation at steady state. Squares: experimental from Ref. [7]. Line: DJS model with $a = 0.3$, $\eta = 0.05$. Both are renormalized by the shear rate $\dot{\gamma}_c$ at the onset of shear banding, and by the value of the stress plateau σ_c. Correspondence is not expected at high shear rates (see main).

further demonstrate the measured lateral velocities to suggest the existence of slow three-dimensional recirculations associated with this instability. To fully connect our results to the studies discussed above, we perform a theoretical analysis of the diffusive Johnson-Segalman (DJS) model in a planar Poiseuille flow and find good quantitative agreement with our experimental results.

Experimental.—We study a semidilute solution of wormlike micelles: CTAB 0.3 M, $NaNO_3$ 0.405 M (Acros organics). Its basic rheology was characterized in Ref. [7], with a stress plateau of 105 Pa beginning at $\dot{\gamma}_c = 5\ s^{-1}$, corresponding to a pressure gradient for the onset of shear banding of $G_b = 3.10^2\ Pa \cdot m^{-1}$. The stress vs strain rate relation renormalized by these parameter values for the onset of shear-banding is shown in Fig. 1(b). In our experimental setup the fluid is driven by a controlled pressure drop in a microchannel of rectangular cross section, with dimensions $(L_x, L_y, L_z) = (5\,cm, 64\ \mu m, 1\,mm)$ with the axes of Fig. 1(a). The photocurable glue used in the fabrication permits high aspect ratio (1:16) channels that do not deform even under pressures far in excess of those in this study [16]. In this work, the setup of [7] has been modified to allow 3D velocity imaging, as follows. Fluorescent tracers of diameter 500 nm are tracked at 50 Hz with a charged coupled device camera through a 100× oil immersion objective mounted on a piezo, giving a 1 μm thick focal plane that can be displaced in y with 10 nm resolution. Image acquisition is performed at a given (x, z) position determined by a moving table. Recorded images have a size $(\Delta x, \Delta z) = (36\ \mu m, 72\ \mu m)$ and correlations are computed on subimages of size 9 μm along z. As a whole, then, a time averaged velocity field can be imaged over the sample with spatial resolution $(\Delta x, \Delta y, \Delta z) = (36\ \mu m, 1\ \mu m, 9\ \mu m)$.

Results.—We measure steady state velocity profiles $v_x(y, z)$ at different downstream locations x, in a cross sectional area [$z = 0$–1 mm] by [$y = 0$–14 μm] shown by the grey rectangle in Fig. 1(a). Figure 2(a) shows such a profile at $x = 4$ cm for a pressure drop $\partial_x p/G_b = 1.3$. It contains the high shear phase close to the bottom wall (dark area) and part of the low shear phase at higher values of y (brighter area). The position of the interface between the bands is extracted from such profiles and its evolution along x is shown in Fig. 2(c). Close to the inlet ($x = 1$ cm) the interface is smooth. The flow profile in this region can be considered a base state from which the instability develops downstream (increasing x). (This occurs via interfacial corrugations that emerge close to the lateral walls, and progressively invade towards the cell center.) The fully developed state [Figs. 2(a) and 2(c) at $x = 4$ cm] has interfacial undulations along z with a wavelength comparable to the channel height L_y. Note that the large aspect ratio $L_z/L_y = 16$ of our flow cell allows us to observe around ten wavelengths in a region that, being well away from the lateral walls, is (*a priori*) translationally invariant in z.

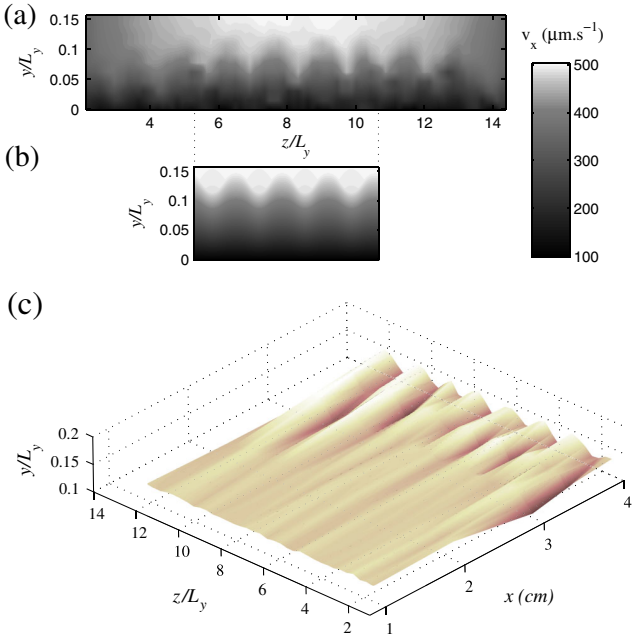

FIG. 2 (color online). (a) Greyscale of the experimental velocity component $v_x(y, z)$ in a subpart of the channel cross section [see Fig. 1(a)], for $\partial_x p/G_b = 1.3$ and $x = 4$ cm, where the instability is fully developed. (b) Corresponding numerical snapshot of the fully developed pattern with $L_z/L_y = 6.0$ and periodic boundaries in z. (c) Spatial evolution of the interface, progressively destabilized along the downstream direction x for $\partial_x p/G_b = 1.3$ at $x = 1$, 2, 3, 3.5 and 4 cm, and obtained from experimental velocity measurements similar to (a).

We now analyze the wavelength $2\pi/q_z$ of these fully developed undulations. For the range of pressure drops explored we find a decreasing wave vector with pressure gradient (Fig. 3 solid symbols), corresponding to a wavelength increase from around 1 to 2 times the height of the channel. The amplitude A of the undulations (Fig. 3 insert) slightly increases with pressure drop and is a few percent of the channel height.

Lateral velocities $v_z(y, z)$ are typically 1% of the $v_x(y, z)$ components and thus comparable to the measurement error. To increase the signal to noise ratio, we sum these velocities over 3 μm thick layers in the height z. Figure 4(a) shows such a profile and the location of the interface for the pressure gradient $\partial_x p/G_b = 1.3$ corresponding to the modulations of $v_x(y, z)$ shown in Fig. 2(a). Though noisy, lateral velocities in the high shear phase are spatially correlated with interface modulations [Fig. 4(c), dots], suggesting the existence of three-dimensional recirculations associated with these.

Comparison with theory.—The DJS model, the details of which are discussed elsewhere [14,17], is not intended to give a microscopically faithful description of our fluid, being, in particular, oversimplified in having a Newtonian high shear branch compared to the sublinear experimental trend [Fig. 1(b)]. It is instead a minimal phenomenological tensorial model that captures the non-

monotonicity of the stress *vs.* strain rate relation [Fig. 1(b)] needed for shear banding, as well as a discontinuity of normal stresses across the interface. Its parameters are solvent viscosity η, slip parameter a, linear modulus G_0, relaxation time τ, and interfacial thickness l. Values for these are guided by previous rheological measurements on this system, independent of the instability studied here. Specifically, the nonlinear flow curve of Fig. 1(b) suggests a ratio $\eta/G_0\tau \approx 0.05$ of high and low shear phase viscosities. We set $a = 0.3$, though our results are robust to reasonable variations in this quantity. A microscopic estimate based on linear rheology leads to $l \approx (k_BT/G_0^{\mathrm{exp}})^{1/3} = O(10^{-8}\ \mathrm{m})$ corresponding to $l/L_y = 0.0015$ [18]. Results are presented by scaling stresses (or pressure drops) and shear rates by their values at the onset of banding, as for the experiments. Our numerical study considers flow driven along a channel by a constant pressure drop, assuming translational invariance of the velocity field in the main flow direction x. The experimental domain well away from the lateral walls is modeled by periodic boundary conditions in z. In each run we evolve the code to steady state $t \to \infty$ with the aim of capturing the flow pattern far downstream from the inlet, assuming that these limits correspond to each other. Linear and nonlinear analyses of the instability are performed with these conditions.

We now compare our experimental and numerical results. First the linear analysis shows the existence of unstable modes with a wave vector oriented in the vorticity direction z. The full nonlinear simulation shows good correspondence with the developed experimental pattern $v_x(y, z)$ at a given pressure gradient [Fig. 2(b)]. The size of the wave vector q_z is furthermore in quantitative agreement between experiment, linear stability analysis and full nonlinear simulations of the final steady state (Fig. 3). Unfortunately, higher values of the pressure drop for which saturation of the wave vector is predicted numerically are unattainable experimentally. Finally, theory indicates the existence of contra-rotary vorticies aligned in the vorticity direction invading the whole height of the channel [Fig. 4(b)]. The signature of these, given by the spatial correlations between lateral velocities and interface position at different heights, is closely identified with its experimental counterpart in Fig. 4(c).

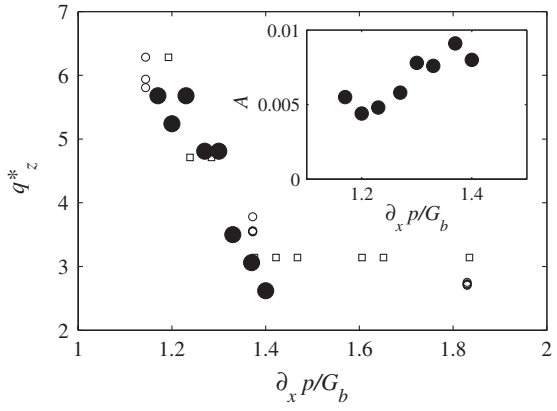

FIG. 3. Wave vector of the interfacial undulations (L_y^{-1} units) as a function of applied pressure drop. Solid circles: experimental. Open squares: fully nonlinear state computed for $L_z/L_y = 4.0$; the numerical wave vector is constrained by the cell length to be heavily quantized as $q_z^\star = 2n\pi/L_z$. Open circles: linear stability analysis of the maximally unstable mode, which does not suffer quantization. Insert: the experimental amplitude A in units of L_y.

Discussion.—We have quantified the spatial features of interfacial modulations that develop in shear-banded flow in a straight microchannel. These have a wave vector in the vorticity direction z, with a wavelength comparable to the channel height $O(100\ \mu\mathrm{m})$. In corresponding conditions, the predictions of the DJS model for this instability are in quantitative agreement with experiment.

Spatial interfacial undulations have been seen previously in the same fluid in a millimetric curved Couette geometry [11,13]. Meanwhile, analysis of the DJS model

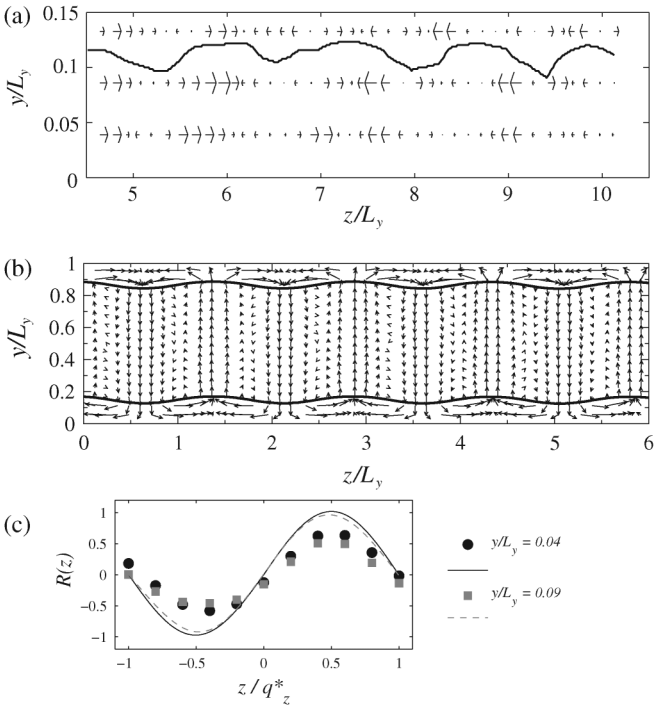

FIG. 4. (a) Experimental lateral components of the velocity $v_z(y, z)$ for $\partial_x p/G_b = 1.3$ in a subsection of the channel cross section at $x = 4$ cm. The maximal velocity represented is $7\ \mu\mathrm{m} \cdot \mathrm{s}^{-1}$. The full line indicates the position of the interface between the two phases. (b) Numerically computed secondary flow field with v_z and v_y components in the whole cross section of the flow, for the same pressure gradient $\partial_x p/G_b = 1.3$ and the same DJS model parameter values as for the numerics of Fig. 2(b). (c) Cross correlation $R(z)$ between the interface position and the lateral velocities $v_z(y, z)$ at different heights y/L_y inside the high shear phase, obtained from experiment data of (a) (symbols) and from simulation data of (b) (lines). Note that in the case of vorticies confined to the high shear phase, $R(z)$ would have opposite values for one of the considered height.

in planar Couette flow predicts an instability driven by a jump in second normal stress across the interface between the bands [15], associated with vortices that invade the whole cell. In contrast, in the experiments of Ref. [13] the vortices appear confined to the high shear phase, suggestive of a different mechanism: a bulk viscoelastic instability of the high shear band, driven by a coupling between cell curvature and first normal stress.

Very recent theory [19] has further predicted a unifying phase diagram that contains both of these instability mechanisms: bulk instability dominates in curved geometries (consistent with the experimental conditions of Ref. [11,13]), while interfacially driven instabilities dominate in rectilinear geometries (consistently with former prediction [15]). Thus, which of these two different mechanisms operates in any given shear-banding flow is predicted to depend on cell curvature. Consequently we believe our straight microchannel flow to be an experimental realization of the interfacially driven viscoelastic instability predicted in Ref. [15], in contrast to the bulk instability of the earlier experiments in curved flow.

A possible alternative explanation of our observations is a subcritical planar viscoelastic instability in the bulk high shear band, of the kind predicted theoretically for a homogeneous base flow in Ref. [20]. (Note that homogeneous planar viscoelastic flows are known to be linearly stable [21].) However, convincing evidence for such instability remains to be found either in computer simulation or experiment. Pending such evidence, we retain the interpretation offered here, based on a supercritical instability arising at the interface between the bands.

We comment now on the value $l = O(10\ \mathrm{nm})$ used numerically. This corresponds to a typical expectation for the correlation length in our fluid [18] and a small value such as this is necessary to predict instability. This differs some from much larger values $l = O(\mu\mathrm{m})$ used to interpret recent experiments [6,12]. However, as suggested in Ref. [12] for cylindrical Couette flows, these larger values could be the outcome of a 1D interpretation of the apparent thickness of a much thinner but spatially undulating interface. Further work is needed to clarify this.

Finally, full linear stability analysis of Poiseuille flow shows the concurrence of unstable q_x and q_z interfacial modes of wavelengths comparable to L_y, over a range of parameter values [22]. Unfortunately our measurement method averages velocities over $\Delta x = 36\ \mu\mathrm{m} > L_y/2$ which precludes observation of q_x. To delineate the effect of nonlinear coupling between these modes is thus an open issue both for theory and experiment.

Conclusion.—We have reported an improved velocimetric technique with finer resolution and 3D mapping, and used it to study the flow of a shear-banding wormlike micellar solution in a microchannel. Our results reveal an interfacial instability with a wave vector in the vorticity direction, in quantitative agreement with a numerical study of the DJS model. The model being highly phenomenological, this agreement suggests robustness of the phenomena to underlying microscopic details, hinging only on the presence of a normal stress jump across the interface between the shear bands. This view is consistent with current progress in the understanding of instabilities in shear-banding fluids, favoring a classical mechanism based on bulk viscoelasticity in the high shear phase in the presence of curvature, in contrast to a different instability mechanism in planar geometries, based on a normal stress jump across the interface, for which our microchannel flow provides an experimental measurement.

Authors acknowledge Mike Cates, Annie Colin, Guillaume Degré, Sandra Lerouge, Alexander Morozov, and Peter Olmsted for discussions; and Total, CNRS, ESPCI and the UK's EPSRC (EP/E5336X/1) for funding.

[1] S. Manneville, Rheol. Acta **47**, 301 (2008); P. D. Olmsted, Rheol. Acta **47**, 283 (2008).
[2] P. Schall and M. van Hecke, Annu. Rev. Fluid Mech. **42**, 67 (2010).
[3] S. Caserta, M. Simeone, and S. Guido, Phys. Rev. Lett. **100**, 137801 (2008).
[4] M. E. Cates and S. M. Fielding, Adv. Phys. **55**, 799 (2006).
[5] R. G. Larson, E. S. G. Shaqfeh, and S. J. Muller, J. Fluid Mech. **218**, 573 (1990).
[6] C. Masselon, J. B. Salmon, and A. Colin, Phys. Rev. Lett. **100**, 038301 (2008).
[7] P. Nghe, G. Degre, P. Tabeling, and A. Ajdari, Appl. Phys. Lett. **93**, 204102 (2008).
[8] M. M. Britton and P. T. Callaghan, Phys. Rev. Lett. **78**, 4930 (1997); P. T. Callaghan, Rheol. Acta **47**, 243 (2008).
[9] J. B. Salmon, A. Colin, S. Manneville, and F. Molino, Phys. Rev. Lett. **90**, 228303 (2003).
[10] S. Manneville, L. Becu, and A. Colin, Eur. Phys. J. Appl. Phys. **28**, 361 (2004).
[11] S. Lerouge, M. Argentina, and J. P. Decruppe, Phys. Rev. Lett. **96**, 088301 (2006).
[12] S. Lerouge, M. A. Fardin, M. Argentina, G. Gregoire, and O. Cardoso, Soft Matter **4**, 1808 (2008).
[13] M. A. Fardin, B. Lasne, O. Cardoso, G. Gregoire, M. Argentina, J. P. Decruppe, and S. Lerouge, Phys. Rev. Lett. **103**, 028302 (2009).
[14] S. M. Fielding, Phys. Rev. Lett. **95**, 134501 (2005).
[15] S. M. Fielding, Phys. Rev. E **76**, 016311 (2007).
[16] D. Bartolo, G. Degre, P. Nghe, and V. Studer, Lab Chip **8**, 274 (2008).
[17] M. W. Johnson and D. Segalman, J. Non-Newtonian Fluid Mech. **2**, 255 (1977); P. D. Olmsted, O. Radulescu, and C. Y. D. Lu, J. Rheol. **44**, 257 (2000).
[18] O. Radulescu, P. D. Olmsted, J. P. Decruppe, S. Lerouge, J. F. Berret, and G. Porte, Europhys. Lett. **62**, 230 (2003).
[19] S. M. Fielding, Phys. Rev. Lett. (to be published).
[20] A. N. Morozov and W. van Saarloos, Phys. Rev. Lett. **95**, 024501 (2005).
[21] T. C. Ho and M. M. Denn, J. Non-Newtonian Fluid Mech. **3**, 179 (1977).
[22] S. M. Fielding and H. Wilson, J. Non-Newtonian Fluid Mech. **165**, 196 (2010).